# Computation of monostatic scattering using the physical optics approximation

Ericsson, Andreas; Sjöberg, Daniel

2017

CODEN:LUTEDX/(TEAT-7255)/1-16/(2017)

# Computation of monostatic scattering using the physical optics approximation

Daniel Sjöberg and Andreas Ericsson

Electromagnetic Theory
Department of Electrical and Information Technology
Lund University
Sweden


(TEAT-7255)/1-16/(2017): D.Sjöberg. Computation of monostatic scattering using the physical optics approximation

Daniel Sjöberg
daniel.sjoberg@eit.lth.se

Andreas Ericsson
andreas.ericsson@eit.lth.se

Department of Electrical and Information Technology
Electromagnetic Theory
Lund University
P.O. Box 118
SE-221 00 Lund
Sweden

This is an author produced preprint version as part of a technical report series from the Electromagnetic Theory group at Lund University, Sweden. Homepage `http://www.eit.lth.se/teat`

Editor: Mats Gustafsson

**Abstract**

We show how to compute the monostatic far field amplitude for an axially symmetric structure illuminated by a plane wave. The resulting expression consists of a line integral of the tangential electric and magnetic fields along the boundary of the scatterer. Simulations are carried out using both a commercial software and an in-house code based on the physical optics approximation. The monostatic scattering from objects, coated with electromagnetic absorbers, is simulated and in the physical optics approximation the absorbers are treated as a local reflection coefficient. This reflection coefficient is dependent on polarization and angle of incidence, and can be computed by a parameter sweep in a full wave simulator such as CST for any type of planar electromagnetic absorber.

# 1 Introduction

Physical optics (PO) is a high frequency approximation method that is used in many applications such as optics, electrical engineering and applied physics [14, 20, 22]. It is an intermediate method between geometrical optics, which treats electromagnetic waves as rays, and full wave electromagnetism [6, 12]. PO is commonly utilized when simulating very large objects without small local details [14, 20].

The approximation consists of estimating the fields on a surface using plane wave representation and scattering, and then integrating the field over the surface to calculate the transmitted or scattered field. This resembles the Born approximation from the fact that details of the problem are treated as perturbations [5]. A strong advantage of this method is the fact that the simulation complexity and computation time does not increase significantly with frequency as in fullwave simulation methods [2, 10, 23]. One drawback with PO is that the accuracy of the method is decreased for scattering in directions other than the specular direction [26]. Modified versions of PO have been presented in the last three decades where this problem has been successfully addressed by utilizing physical theory of diffraction (PTD) [18, 24, 25]. Furthermore, by utilizing a multilevel computational sequence based on hierarchical decomposition of the radiating aperture, the accuracy and computation speed of PO has been significantly improved for bistatic and non-specular reflections [3, 4, 11, 16, 17, 21, 26].

Throughout the years, PO has been heavily relied on for calculating the scattered fields from PEC objects. But in [1, 27], the method was used to model conductive objects coated by for example radar absorbing materials (RAM). This type of simulation problems imply very slow and computationally heavy simulations in a full wave solver. In PO however, adding a RAM to the scatterer results in practically no increase in computation time in comparison to simulating a PEC object. For canonical structures, such as a layered sphere, the scattering problem can be solved analytically for scatterers up to hundreds of wavelengths in size. In [8, 9], a PEC sphere coated by different types of electromagnetic absorbers were simulated in order to evaluate the effect of curvature on the absorber performance. The PO approximation can be used to extend this study to scatterers of general shape.

In this work, integral expressions are derived for calculating the monostatic scattering from axially symmetric and general objects in free space. The PO approximation is utilized to achieve fast calculations of the monostatic scattering from perfect electric conducting (PEC) objects coated by an electromagnetic absorber. The absorber is treated as an angle of incidence dependent reflection dyadic at the surface of the scatterer. The time convention $\mathrm{e}^{\mathrm{j}\omega t}$ is used throughout this work, and the derived expressions presented herein are used in [7] for RCS reduction of a number of different scatterers.

This report is organized as follows: in Section 2 the PO approximation is described in detail, both for general and axially symmetric scatterers. An integral expression for calculating the monostatic scattering from an axially-symmetric object, illuminated parallel to its axis of rotation, is presented in Section 3. This expression can be used in any solver as long as the electric and magnetic fields are known at a surface enclosing the scatterer. In Section 4 simulation results are presented of the monostatic scattering from an axially symmetric scatterer, illuminated both along the axis of rotation and off-axis. Finally, some concluding remarks are presented in Section 5.

# 2 Physical optics approximation

## 2.1 General formulation

In the physical optics (PO) approximation, the scattering surface is assumed to be locally flat and described by a reflection matrix so that the tangential electric and magnetic fields are given by

$$\boldsymbol{E}_{\mathrm{t}} = (\mathbf{I} + \mathbf{R}) \cdot \boldsymbol{E}_{\mathrm{t}}^{(\mathrm{i})} \tag{2.1}$$

$$\boldsymbol{H}_{\mathrm{t}} = \mathbf{Z}_{\mathrm{w}}^{-1} \cdot (\mathbf{I} - \mathbf{R}) \cdot \boldsymbol{E}_{\mathrm{t}}^{(\mathrm{i})} \tag{2.2}$$

Using the unit vectors $\hat{\boldsymbol{p}}$ and $\hat{\boldsymbol{s}}$ spanning the surface, we can write $\mathbf{I} = \hat{\boldsymbol{p}}\hat{\boldsymbol{p}} + \hat{\boldsymbol{s}}\hat{\boldsymbol{s}}$ to denote the identity matrix in the tangential plane of the surface, whereas $\mathbf{R}$ denotes the reflection matrix, and $\mathbf{Z}_{\mathrm{w}}^{-1}$ is the wave admittance matrix of the surrounding medium. This is defined as follows. A plane wave propagating in free space in the $\hat{\boldsymbol{k}}$ direction is given by the right-hand rule as $\boldsymbol{E} = \boldsymbol{E}_0 \mathrm{e}^{-\mathrm{j}k\hat{\boldsymbol{k}}\cdot\boldsymbol{r}}$ and $\boldsymbol{H} = \eta_0^{-1}\hat{\boldsymbol{k}} \times \boldsymbol{E}_0 \mathrm{e}^{-\mathrm{j}k\hat{\boldsymbol{k}}\cdot\boldsymbol{r}}$, where $\eta_0$ is the wave impedance in vacuum. Now fix a different direction $\hat{\boldsymbol{u}}$, and consider the components of $\boldsymbol{E}$ and $\boldsymbol{H}$ orthogonal to $\hat{\boldsymbol{u}}$ (the transverse parts, $\boldsymbol{E}_{\mathrm{t}}$ and $\boldsymbol{H}_{\mathrm{t}}$). The wave admittance is then defined by the relation $\boldsymbol{H}_{\mathrm{t}} = \mathrm{sign}(\hat{\boldsymbol{u}} \cdot \hat{\boldsymbol{k}})\mathbf{Z}_{\mathrm{w}}^{-1} \cdot \boldsymbol{E}_{\mathrm{t}}$. In this case, it can be represented as (with $\hat{\boldsymbol{u}} = -\hat{\boldsymbol{n}}$ and assuming $(\hat{\boldsymbol{p}}, \hat{\boldsymbol{s}}, \hat{\boldsymbol{n}})$ is a right-handed system and $\hat{\boldsymbol{n}}$ is the outward pointing normal)

$$\mathbf{Z}_{\mathrm{w}}^{-1} = -\hat{\boldsymbol{n}} \times \eta_0^{-1} \left( \frac{1}{\cos\theta} \hat{\boldsymbol{p}}\hat{\boldsymbol{p}} + \cos\theta \hat{\boldsymbol{s}}\hat{\boldsymbol{s}} \right) = \eta_0^{-1} \left( \frac{-1}{\cos\theta} \hat{\boldsymbol{s}}\hat{\boldsymbol{p}} + \cos\theta \hat{\boldsymbol{p}}\hat{\boldsymbol{s}} \right) \tag{2.3}$$

Here, $\eta_0$ is the wave impedance in vacuum and $\theta$ is the angle of incidence. For an isotropic case, the reflection matrix can be represented as

$$\mathbf{R} = R_{\mathrm{TM}}(\theta)\hat{\boldsymbol{p}}\hat{\boldsymbol{p}} + R_{\mathrm{TE}}(\theta)\hat{\boldsymbol{s}}\hat{\boldsymbol{s}} \tag{2.4}$$

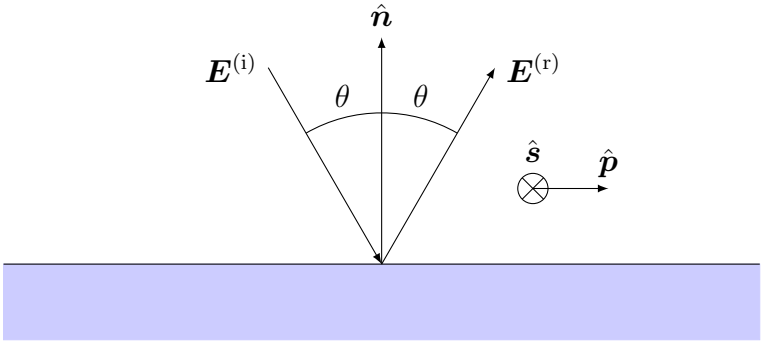


Figure 1: Local geometry of the plane of incidence, defining the unit vectors $\hat{\boldsymbol{p}}$ (corresponding to TM polarization) and $\hat{\boldsymbol{s}}$ (corresponding to TE polarization).

and we have the result

$$\boldsymbol{E}_{\mathrm{t}} = (1 + R_{\mathrm{TM}}(\theta))E^{(\mathrm{i})}_{\mathrm{TM}}\hat{\boldsymbol{p}} + (1 + R_{\mathrm{TE}}(\theta))E^{(\mathrm{i})}_{\mathrm{TE}}\hat{\boldsymbol{s}} \tag{2.5}$$

$$\boldsymbol{H}_{\mathrm{t}} = -\frac{\eta_0^{-1}}{\cos\theta}(1 - R_{\mathrm{TM}}(\theta))E^{(\mathrm{i})}_{\mathrm{TM}}\hat{\boldsymbol{s}} + \eta_0^{-1}\cos\theta(1 - R_{\mathrm{TE}}(\theta))E^{(\mathrm{i})}_{\mathrm{TE}}\hat{\boldsymbol{p}} \tag{2.6}$$

Note the switched role between TM/TE and $\hat{\boldsymbol{p}}/\hat{\boldsymbol{s}}$ for the magnetic fields. Also note that the idea of an incident and reflected field is only valid when $\cos\theta = \hat{\boldsymbol{u}} \cdot \hat{\boldsymbol{k}} = -\hat{\boldsymbol{n}} \cdot \hat{\boldsymbol{k}} > 0$. If this is not satisfied, the incident wave is coming from below, that is, we are in the shadow zone of the structure. This means we should set $\boldsymbol{E}_{\mathrm{t}}$ and $\boldsymbol{H}_{\mathrm{t}}$ to zero whenever $\cos\theta \leq 0$.

Since the incident field components are $E^{(\mathrm{i})}_{\mathrm{TM}} = \hat{\boldsymbol{p}} \cdot \boldsymbol{E}^{(\mathrm{i})}$ and $E^{(\mathrm{i})}_{\mathrm{TE}} = \hat{\boldsymbol{s}} \cdot \boldsymbol{E}^{(\mathrm{i})}$, we can write

$$\begin{aligned}\boldsymbol{E} \times \hat{\boldsymbol{n}} = -\hat{\boldsymbol{n}} \times \boldsymbol{E}_{\mathrm{t}} &= -(1 + R_{\mathrm{TM}}(\theta))E^{(\mathrm{i})}_{\mathrm{TM}}\hat{\boldsymbol{s}} + (1 + R_{\mathrm{TE}}(\theta))E^{(\mathrm{i})}_{\mathrm{TE}}\hat{\boldsymbol{p}} \\ &= [-(1 + R_{\mathrm{TM}}(\theta))\hat{\boldsymbol{s}}\hat{\boldsymbol{p}} + (1 + R_{\mathrm{TE}}(\theta))\hat{\boldsymbol{p}}\hat{\boldsymbol{s}}] \cdot \boldsymbol{E}^{(\mathrm{i})}\end{aligned} \tag{2.7}$$

and

$$\begin{aligned}\hat{\boldsymbol{n}} \times \boldsymbol{H} = \hat{\boldsymbol{n}} \times \boldsymbol{H}_{\mathrm{t}} &= \frac{\eta_0^{-1}}{\cos\theta}(1 - R_{\mathrm{TM}}(\theta))E^{(\mathrm{i})}_{\mathrm{TM}}\hat{\boldsymbol{p}} + \eta_0^{-1}\cos\theta(1 - R_{\mathrm{TE}}(\theta))E^{(\mathrm{i})}_{\mathrm{TE}}\hat{\boldsymbol{s}} \\ &= \left[\frac{\eta_0^{-1}}{\cos\theta}(1 - R_{\mathrm{TM}}(\theta))\hat{\boldsymbol{p}}\hat{\boldsymbol{p}} + \eta_0^{-1}\cos\theta(1 - R_{\mathrm{TE}}(\theta))\hat{\boldsymbol{s}}\hat{\boldsymbol{s}}\right] \cdot \boldsymbol{E}^{(\mathrm{i})}\end{aligned} \tag{2.8}$$

With $\boldsymbol{E}^{(\mathrm{i})} = \boldsymbol{E}_0 \mathrm{e}^{-\mathrm{j}k\hat{\boldsymbol{k}}\cdot\boldsymbol{r}}$ and the observation direction $\hat{\boldsymbol{r}} = -\hat{\boldsymbol{k}}$, the far field amplitude is defined in [15, p.198] as

$$\begin{aligned}\boldsymbol{F}(-\hat{\boldsymbol{k}}) &= -\frac{\mathrm{j}k}{4\pi}\hat{\boldsymbol{k}} \times \int_S \left[\boldsymbol{E}(\boldsymbol{r}) \times \hat{\boldsymbol{n}} - \eta_0\hat{\boldsymbol{k}} \times (\hat{\boldsymbol{n}} \times \boldsymbol{H}(\boldsymbol{r}))\right] \mathrm{e}^{-\mathrm{j}k\hat{\boldsymbol{k}}\cdot\boldsymbol{r}}\,\mathrm{d}S \\ &= -\frac{\mathrm{j}k}{4\pi}\hat{\boldsymbol{k}} \times \int_S \Bigg\{ [-(1 + R_{\mathrm{TM}}(\theta))\hat{\boldsymbol{s}}\hat{\boldsymbol{p}} + (1 + R_{\mathrm{TE}}(\theta))\hat{\boldsymbol{p}}\hat{\boldsymbol{s}}] \\ &\quad - \hat{\boldsymbol{k}} \times \left[\frac{1}{\cos\theta}(1 - R_{\mathrm{TM}}(\theta))\hat{\boldsymbol{p}}\hat{\boldsymbol{p}} + \cos\theta(1 - R_{\mathrm{TE}}(\theta))\hat{\boldsymbol{s}}\hat{\boldsymbol{s}}\right] \Bigg\} \cdot \boldsymbol{E}_0 \mathrm{e}^{-2\mathrm{j}k\hat{\boldsymbol{k}}\cdot\boldsymbol{r}}\,\mathrm{d}S\end{aligned} \tag{2.9}$$

Thus, what is needed to compute the integral is mostly a geometric analysis of the surface so that the basis vectors $\hat{\boldsymbol{p}}$ and $\hat{\boldsymbol{s}}$ can be computed.

Note that the idea of an incident and reflected field is only valid when $\cos\theta = -\hat{\boldsymbol{n}} \cdot \hat{\boldsymbol{k}} > 0$. If this is not satisfied, the incident wave is coming from below, that is, we are in the shadow zone of the structure. This means the integrand is set to zero on the parts of $S$ where $\cos\theta \leq 0$.

## 2.2 parametrization of general scatterers

Assume the surface $S$ can be parametrized by two real scalars $u$ and $v$:

$$S = \{\boldsymbol{r}(u,v) : \ a < u < b,\, c < v < d\} \tag{2.10}$$

where $\boldsymbol{r}(u,v) = x(u,v)\hat{\boldsymbol{x}} + y(u,v)\hat{\boldsymbol{y}} + z(u,v)\hat{\boldsymbol{z}}$. A local tangential basis (not necessarily orthogonal), and the unit vector, can be found from

$$\hat{\boldsymbol{u}} = \frac{\boldsymbol{r}_u}{|\boldsymbol{r}_u|} = \frac{x_u\hat{\boldsymbol{x}} + y_u\hat{\boldsymbol{y}} + z_u\hat{\boldsymbol{z}}}{\sqrt{x_u^2 + y_u^2 + z_u^2}} \tag{2.11}$$

$$\hat{\boldsymbol{v}} = \frac{\boldsymbol{r}_v}{|\boldsymbol{r}_v|} = \frac{x_v\hat{\boldsymbol{x}} + y_v\hat{\boldsymbol{y}} + z_v\hat{\boldsymbol{z}}}{\sqrt{x_v^2 + y_v^2 + z_v^2}} \tag{2.12}$$

$$\hat{\boldsymbol{n}} = \frac{\hat{\boldsymbol{u}} \times \hat{\boldsymbol{v}}}{|\hat{\boldsymbol{u}} \times \hat{\boldsymbol{v}}|} \tag{2.13}$$

where the index denotes partial differentiation, and we assume the parametrization has been chosen such that $\hat{\boldsymbol{n}}$ is pointing out of the structure.

The plane of incidence is spanned by $\hat{\boldsymbol{n}}$ and $\hat{\boldsymbol{k}}$. The TE and TM directions are found from

$$\hat{\boldsymbol{s}} = \frac{\hat{\boldsymbol{n}} \times \hat{\boldsymbol{k}}}{|\hat{\boldsymbol{n}} \times \hat{\boldsymbol{k}}|} \qquad\qquad \hat{\boldsymbol{p}} = \hat{\boldsymbol{s}} \times \hat{\boldsymbol{n}} \tag{2.14}$$

If $\hat{\boldsymbol{k}} \times \hat{\boldsymbol{n}} = \boldsymbol{0}$ then $\hat{\boldsymbol{p}}$ and $\hat{\boldsymbol{s}}$ are arbitrary. The angle of incidence is found from

$$\cos\theta = -\hat{\boldsymbol{n}} \cdot \hat{\boldsymbol{k}} \tag{2.15}$$

and the surface element is $\mathrm{d}S = |\boldsymbol{r}_u \times \boldsymbol{r}_v|\,\mathrm{d}u\,\mathrm{d}v$.

## 2.3 Parametrization of axially symmetric scatterers

Assume the curve $\gamma$ defines an axially symmetric scatterer, as in Figure 2, that can be parametrized by a real scalar $u$:

$$\gamma = \{\boldsymbol{r}(u) : \ a < u < b\} \tag{2.16}$$

where $\boldsymbol{r}(u) = \rho(u)\hat{\boldsymbol{\rho}} + z(u)\hat{\boldsymbol{z}}$. The start point is given by $\boldsymbol{r}(a)$ and the end point by $\boldsymbol{r}(b)$. A local tangential basis is in this case given by (where $\hat{\boldsymbol{\varphi}}$ is the direction of

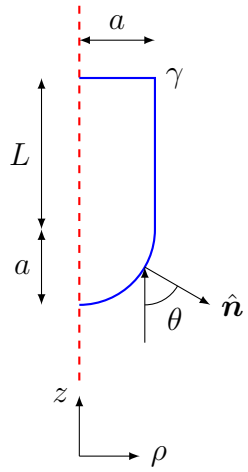


Figure 2: A typical geometry, with a hemispherically capped right circular cylinder of height $L$ and radius $a$. The total height is $L + a$.

increasing azimuth angle $\varphi$)

$$\hat{\boldsymbol{u}} = \frac{\boldsymbol{r}_u}{|\boldsymbol{r}_u|} = \rho'(u)\hat{\boldsymbol{\rho}} + z'(u)\hat{\boldsymbol{z}} \tag{2.17}$$

$$\hat{\boldsymbol{v}} = \frac{\boldsymbol{r}_v}{|\boldsymbol{r}_v|} = \hat{\boldsymbol{\varphi}} \tag{2.18}$$

$$\hat{\boldsymbol{n}} = \frac{\hat{\boldsymbol{u}} \times \hat{\boldsymbol{v}}}{|\hat{\boldsymbol{u}} \times \hat{\boldsymbol{v}}|} = \frac{z'(u)\hat{\boldsymbol{\rho}} - \rho'(u)\hat{\boldsymbol{z}}}{\sqrt{(z'(u))^2 + (\rho'(u))^2}} \tag{2.19}$$

where the index denotes partial differentiation, and we assume the parametrization has been chosen such that $\hat{\boldsymbol{n}}$ pointing out of the structure (in the typical case, we have $z'(u) \geq 0$). The length element is $\mathrm{d}\ell = (\mathrm{d}\ell/\,\mathrm{d}u)\,\mathrm{d}u$, where

$$\frac{\mathrm{d}\ell}{\mathrm{d}u} = \sqrt{(z'(u))^2 + (\rho'(u))^2} \tag{2.20}$$

and the angle of incidence is given by $\cos\theta = -\hat{\boldsymbol{k}} \cdot \hat{\boldsymbol{n}}(u)$. The TE and TM directions are, also in this case, found from

$$\hat{\boldsymbol{s}} = \frac{\hat{\boldsymbol{n}} \times \hat{\boldsymbol{k}}}{|\hat{\boldsymbol{n}} \times \hat{\boldsymbol{k}}|} \qquad\qquad \hat{\boldsymbol{p}} = \hat{\boldsymbol{s}} \times \hat{\boldsymbol{n}} \tag{2.21}$$

# 3 Monostatic RCS from axially symmetric scatterers, on-axis illumination

In this section an expression for calculating the monostatic far field amplitude from axially symmetric scatterers, illuminated parallel to the axis of rotation, is presented. From this expression the monostatic RCS can be determined taking the symmetry of the situation into account, either in a commercial full wave solver or in a PO implementation.

## 3.1 The far field integral

The far field amplitude from tangential electric and magnetic fields on a general surface $S$ is defined in [15, p.198] as

$$\boldsymbol{F}(\hat{\boldsymbol{r}}) = \frac{\mathrm{j}k}{4\pi}\hat{\boldsymbol{r}} \times \int_S [\boldsymbol{E}(\boldsymbol{r}') \times \hat{\boldsymbol{n}} + \eta_0 \hat{\boldsymbol{r}} \times (\hat{\boldsymbol{n}} \times \boldsymbol{H}(\boldsymbol{r}'))] \, \mathrm{e}^{\mathrm{j}k\hat{\boldsymbol{r}}\cdot\boldsymbol{r}'} \, \mathrm{d}S' \tag{3.1}$$

For any scatterer the fields can be represented in cylindrical coordinates $(\rho, \varphi, z)$ as

$$\boldsymbol{E}(\boldsymbol{r}) = \sum_{m=-\infty}^{\infty} \left[E_\rho^{(m)}(\rho,z)\hat{\boldsymbol{\rho}} + E_\varphi^{(m)}(\rho,z)\hat{\boldsymbol{\varphi}} + E_z^{(m)}(\rho,z)\hat{\boldsymbol{z}}\right] \mathrm{e}^{-\mathrm{j}m\varphi} \tag{3.2}$$

$$\boldsymbol{H}(\boldsymbol{r}) = \sum_{m=-\infty}^{\infty} \left[H_\rho^{(m)}(\rho,z)\hat{\boldsymbol{\rho}} + H_\varphi^{(m)}(\rho,z)\hat{\boldsymbol{\varphi}} + H_z^{(m)}(\rho,z)\hat{\boldsymbol{z}}\right] \mathrm{e}^{-\mathrm{j}m\varphi} \tag{3.3}$$

For an axially symmetric scatterer, numerical methods typically fix the azimuthal mode index $m$ and solve for the electric field components $(E_\rho^{(m)}(\rho,z), ...)$ and the corresponding magnetic field components. The curl operation can be written in cylindrical coordinates as

$$\nabla \times \boldsymbol{E} = \hat{\boldsymbol{\rho}}\left(\frac{1}{\rho}\frac{\partial E_z}{\partial \varphi} - \frac{\partial E_\varphi}{\partial z}\right) + \hat{\boldsymbol{\varphi}}\left(\frac{\partial E_\rho}{\partial z} - \frac{\partial E_z}{\partial \rho}\right) + \hat{\boldsymbol{z}}\left(\frac{1}{\rho}\frac{\partial}{\partial \rho}(\rho E_\varphi) - \frac{1}{\rho}\frac{\partial E_\rho}{\partial \varphi}\right) \tag{3.4}$$

Maxwell's equations in free space, $\nabla \times \boldsymbol{E} = -\mathrm{j}\omega\mu_0\boldsymbol{H}$ and $\nabla \times \boldsymbol{H} = \mathrm{j}\omega\epsilon_0\boldsymbol{E}$, can then be written

$$-\frac{\mathrm{j}m}{\rho}E_z^{(m)} - \frac{\partial E_\varphi^{(m)}}{\partial z} = -\mathrm{j}\omega\mu_0 H_\rho^{(m)} \qquad -\frac{\mathrm{j}m}{\rho}H_z^{(m)} - \frac{\partial H_\varphi^{(m)}}{\partial z} = \mathrm{j}\omega\epsilon_0 E_\rho^{(m)} \tag{3.5}$$

$$\frac{\partial E_\rho^{(m)}}{\partial z} - \frac{\partial E_z^{(m)}}{\partial \rho} = -\mathrm{j}\omega\mu_0 H_\varphi^{(m)} \qquad \frac{\partial H_\rho^{(m)}}{\partial z} - \frac{\partial H_z^{(m)}}{\partial \rho} = \mathrm{j}\omega\epsilon_0 E_\varphi^{(m)} \tag{3.6}$$

$$\frac{1}{\rho}\frac{\partial}{\partial \rho}(\rho E_\varphi^{(m)}) + \frac{\mathrm{j}m}{\rho}E_\rho^{(m)} = -\mathrm{j}\omega\mu_0 H_z^{(m)} \quad \frac{1}{\rho}\frac{\partial}{\partial \rho}(\rho H_\varphi^{(m)}) + \frac{\mathrm{j}m}{\rho}H_\rho^{(m)} = \mathrm{j}\omega\epsilon_0 E_z^{(m)} \tag{3.7}$$

It is seen that only for $m = 0$ do these equations split into an in-plane electric field mode $(E_\rho^{(0)}, E_z^{(0)}, H_\varphi^{(0)})$, and an out-of-plane electric field mode $(E_\varphi^{(0)}, H_\rho^{(0)}, H_z^{(0)})$. For $m \neq 0$, we need to solve for all field components.

The unit normal vector is $\hat{\boldsymbol{n}} = n_\rho\hat{\boldsymbol{\rho}} + n_z\hat{\boldsymbol{z}}$, meaning the electric and magnetic tangential currents are (using $\hat{\boldsymbol{\rho}} \times \hat{\boldsymbol{\varphi}} = \hat{\boldsymbol{z}}$)

$$\boldsymbol{E}^{(m)} \times \hat{\boldsymbol{n}} = (n_\rho E_z^{(m)} - n_z E_\rho^{(m)})\hat{\boldsymbol{\varphi}} - n_\rho E_\varphi^{(m)}\hat{\boldsymbol{z}} + n_z E_\varphi^{(m)}\hat{\boldsymbol{\rho}} \tag{3.8}$$

$$\hat{\boldsymbol{n}} \times \boldsymbol{H}^{(m)} = (-n_\rho H_z^{(m)} + n_z H_\rho^{(m)})\hat{\boldsymbol{\varphi}} + n_\rho H_\varphi^{(m)}\hat{\boldsymbol{z}} - n_z H_\varphi^{(m)}\hat{\boldsymbol{\rho}} \tag{3.9}$$

Choosing the observation direction $\hat{\boldsymbol{r}} = -\hat{\boldsymbol{z}}$, all $z$-components will disappear due to the cross products with $\hat{\boldsymbol{z}}$. The typical integral for computing the far field is then

$$\int_\gamma \int_{\varphi=0}^{2\pi} \left[(n_\rho E_z^{(m)}(\rho,z) - n_z E_\rho^{(m)}(\rho,z))\hat{\boldsymbol{\varphi}} + n_z E_\varphi^{(m)}(\rho,z)\hat{\boldsymbol{\rho}}\right] \mathrm{e}^{-\mathrm{j}m\varphi}\mathrm{e}^{-\mathrm{j}kz}\rho \, \mathrm{d}\varphi \, \mathrm{d}\ell \tag{3.10}$$

where $\gamma$ is the curve in the $\rho$-$z$ plane describing the object, as in Figure 2, and $\rho$ and $z$ are computed on this curve, with $\mathrm{d}\ell$ as a line element. The unit vectors are

$$\hat{\boldsymbol{\rho}} = \hat{\boldsymbol{x}}\cos\varphi + \hat{\boldsymbol{y}}\sin\varphi \tag{3.11}$$
$$\hat{\boldsymbol{\varphi}} = -\hat{\boldsymbol{x}}\sin\varphi + \hat{\boldsymbol{y}}\cos\varphi \tag{3.12}$$

We have the orthogonalities

$$\int_0^{2\pi} \cos\varphi \mathrm{e}^{-\mathrm{j}m\varphi}\,\mathrm{d}\varphi = \pi\delta_{m,1} + \pi\delta_{m,-1} \tag{3.13}$$
$$\int_0^{2\pi} \sin\varphi \mathrm{e}^{-\mathrm{j}m\varphi}\,\mathrm{d}\varphi = -\mathrm{j}\pi\delta_{m,1} + \mathrm{j}\pi\delta_{m,-1} \tag{3.14}$$

which means only $m = \pm 1$ contributes, and we have

$$\begin{aligned}
&\int_{\varphi=0}^{2\pi} \left[(n_\rho E_z^{(m)}(\rho,z) - n_z E_\rho^{(m)}(\rho,z))\hat{\boldsymbol{\varphi}} + n_z E_\varphi^{(m)}(\rho,z)\hat{\boldsymbol{\rho}}\right] \mathrm{e}^{-\mathrm{j}m\varphi}\,\mathrm{d}\varphi \\
&\quad = (n_\rho E_z^{(m)}(\rho,z) - n_z E_\rho^{(m)}(\rho,z))\pi[\mathrm{j}\hat{\boldsymbol{x}}(\delta_{m,1} - \delta_{m,-1}) + \hat{\boldsymbol{y}}(\delta_{m,1} + \delta_{m,-1}] \\
&\qquad + n_z E_\varphi^{(m)}(\rho,z)\pi[\hat{\boldsymbol{x}}(\delta_{m,1} + \delta_{m,-1}) + \mathrm{j}\hat{\boldsymbol{y}}(-\delta_{m,1} + \delta_{m,-1})]
\end{aligned} \tag{3.15}$$

The magnetic field has an extra vector multiplication with $-\hat{\boldsymbol{z}}$:

$$\begin{aligned}
&-\hat{\boldsymbol{z}} \times \int_0^{2\pi} \hat{\boldsymbol{n}} \times \boldsymbol{H}^{(m)} \mathrm{e}^{-\mathrm{j}m\varphi}\,\mathrm{d}\varphi = \hat{\boldsymbol{z}} \times \int_0^{2\pi} \boldsymbol{H}^{(m)} \times \hat{\boldsymbol{n}} \mathrm{e}^{-\mathrm{j}m\varphi}\,\mathrm{d}\varphi \\
&\quad = (n_\rho H_z^{(m)}(\rho,z) - n_z H_\rho^{(m)}(\rho,z))\pi\hat{\boldsymbol{z}} \times [\mathrm{j}\hat{\boldsymbol{x}}(\delta_{m,1} - \delta_{m,-1}) + \hat{\boldsymbol{y}}(\delta_{m,1} + \delta_{m,-1}] \\
&\qquad + n_z H_\varphi^{(m)}(\rho,z)\pi\hat{\boldsymbol{z}} \times [\hat{\boldsymbol{x}}(\delta_{m,1} + \delta_{m,-1}) + \mathrm{j}\hat{\boldsymbol{y}}(-\delta_{m,1} + \delta_{m,-1})] \\
&\quad = (n_\rho H_z^{(m)}(\rho,z) - n_z H_\rho^{(m)}(\rho,z))\pi[\mathrm{j}\hat{\boldsymbol{y}}(\delta_{m,1} - \delta_{m,-1}) - \hat{\boldsymbol{x}}(\delta_{m,1} + \delta_{m,-1}] \\
&\qquad + n_z H_\varphi^{(m)}(\rho,z)\pi[\hat{\boldsymbol{y}}(\delta_{m,1} + \delta_{m,-1}) + \mathrm{j}\hat{\boldsymbol{x}}(\delta_{m,1} - \delta_{m,-1})]
\end{aligned} \tag{3.16}$$

Let $\boldsymbol{F}^\pm(-\hat{\boldsymbol{z}})$ denote the far field amplitude for $m = \pm 1$. We then have

$$\begin{aligned}
&\boldsymbol{F}^\pm(-\hat{\boldsymbol{z}}) = -\frac{\mathrm{j}k}{4\pi}\hat{\boldsymbol{z}} \times \int_S \left[\boldsymbol{E}^\pm(\boldsymbol{r}) \times \hat{\boldsymbol{n}} - \eta_0 \hat{\boldsymbol{z}} \times (\hat{\boldsymbol{n}} \times \boldsymbol{H}^\pm(\boldsymbol{r}))\right] \mathrm{e}^{\mp\mathrm{j}\varphi}\mathrm{e}^{-\mathrm{j}kz}\,\mathrm{d}S \\
&\quad = -\frac{\mathrm{j}k}{4\pi}\hat{\boldsymbol{z}} \times \int_\gamma \Big[(n_\rho E_z^\pm(\rho,z) - n_z E_\rho^\pm(\rho,z))\pi[\pm\mathrm{j}\hat{\boldsymbol{x}} + \hat{\boldsymbol{y}}] + n_z E_\varphi^\pm(\rho,z)\pi[\hat{\boldsymbol{x}} \mp \mathrm{j}\hat{\boldsymbol{y}}] \\
&\qquad + \eta_0(n_\rho H_z^\pm(\rho,z) - n_z H_\rho^\pm(\rho,z))\pi[\pm\mathrm{j}\hat{\boldsymbol{y}} - \hat{\boldsymbol{x}}] + \eta_0 n_z H_\varphi^\pm(\rho,z)\pi[\hat{\boldsymbol{y}} \pm \mathrm{j}\hat{\boldsymbol{x}}]\Big] \mathrm{e}^{-\mathrm{j}kz}\rho\,\mathrm{d}\ell \\
&\quad = -\frac{\mathrm{j}k}{4}\int_\gamma \Big[(n_\rho E_z^\pm(\rho,z) - n_z E_\rho^\pm(\rho,z))[\pm\mathrm{j}\hat{\boldsymbol{y}} - \hat{\boldsymbol{x}}] + n_z E_\varphi^\pm(\rho,z)[\hat{\boldsymbol{y}} \pm \mathrm{j}\hat{\boldsymbol{x}}] \\
&\qquad + \eta_0(n_\rho H_z^\pm(\rho,z) - n_z H_\rho^\pm(\rho,z))[\mp\mathrm{j}\hat{\boldsymbol{x}} - \hat{\boldsymbol{y}}] + \eta_0 n_z H_\varphi^\pm(\rho,z)[-\hat{\boldsymbol{x}} \pm \mathrm{j}\hat{\boldsymbol{y}}]\Big] \mathrm{e}^{-\mathrm{j}kz}\rho\,\mathrm{d}\ell
\end{aligned} \tag{3.17}$$

Let the ± modes be excited by

$$\begin{aligned}\boldsymbol{E}_0^{\pm} &= E_0(\hat{\boldsymbol{\rho}} \mp \mathrm{j}\hat{\boldsymbol{\varphi}})\mathrm{e}^{\mp\mathrm{j}\varphi} = E_0(\hat{\boldsymbol{x}}\cos\varphi + \hat{\boldsymbol{y}}\sin\varphi \mp \mathrm{j}(-\hat{\boldsymbol{x}}\sin\varphi + \hat{\boldsymbol{y}}\cos\varphi))\mathrm{e}^{\mp\mathrm{j}\varphi} \\ &= E_0(\hat{\boldsymbol{x}}(\cos\varphi \pm \mathrm{j}\sin\varphi) \mp \mathrm{j}\hat{\boldsymbol{y}}(\cos\varphi \pm \mathrm{j}\sin\varphi)\mathrm{e}^{\mp\mathrm{j}\varphi} = E_0(\hat{\boldsymbol{x}}\mathrm{e}^{\pm\mathrm{j}\varphi} \mp \mathrm{j}\hat{\boldsymbol{y}}\mathrm{e}^{\pm\mathrm{j}\varphi})\mathrm{e}^{\mp\mathrm{j}\varphi} \\ &= E_0(\hat{\boldsymbol{x}} \mp \mathrm{j}\hat{\boldsymbol{y}}) \quad (3.18)\end{aligned}$$

which is a right/left-hand circularly polarized plane wave. As can be seen from equations (3.5), (3.6), and (3.7), the resulting ± modes then have the following parity:

$$(E_\rho^+, E_z^+, H_\varphi^+) = (E_\rho^-, E_z^-, H_\varphi^-) \quad (3.19)$$

$$(E_\varphi^+, H_\rho^+, H_z^+) = -(E_\varphi^-, H_\rho^-, H_z^-) \quad (3.20)$$

and we find

$$\begin{aligned}\boldsymbol{F}^{\pm}(-\hat{\boldsymbol{z}}) = -\frac{\mathrm{j}k}{4}\int_\gamma \Big[&(n_\rho E_z^+(\rho,z) - n_z E_\rho^+(\rho,z))[\pm\mathrm{j}\hat{\boldsymbol{y}} - \hat{\boldsymbol{x}}] \pm n_z E_\varphi^+(\rho,z)[\hat{\boldsymbol{y}} \pm \mathrm{j}\hat{\boldsymbol{x}}] \\ &\pm \eta_0(n_\rho H_z^+(\rho,z) - n_z H_\rho^+(\rho,z))[\mp\mathrm{j}\hat{\boldsymbol{x}} - \hat{\boldsymbol{y}}] + \eta_0 n_z H_\varphi^+(\rho,z)[-\hat{\boldsymbol{x}} \pm \mathrm{j}\hat{\boldsymbol{y}}]\Big]\mathrm{e}^{-\mathrm{j}kz}\rho\,\mathrm{d}\ell\end{aligned} \quad (3.21)$$

The far field amplitude corresponding to an incident linearly polarized plane wave, $(\boldsymbol{E}_0^+ + \boldsymbol{E}_0^-)/2 = E_0\hat{\boldsymbol{x}}$, is then

$$\begin{aligned}\frac{\boldsymbol{F}^+(-\hat{\boldsymbol{z}}) + \boldsymbol{F}^-(-\hat{\boldsymbol{z}})}{2} &= -\frac{\mathrm{j}k}{4}\int_\gamma \Big[(n_\rho E_z^+(\rho,z) - n_z E_\rho^+(\rho,z))[-\hat{\boldsymbol{x}}] + n_z E_\varphi^+(\rho,z)[\mathrm{j}\hat{\boldsymbol{x}}] \\ &\quad + \eta_0(n_\rho H_z^+(\rho,z) - n_z H_\rho^+(\rho,z))[-\mathrm{j}\hat{\boldsymbol{x}}] + \eta_0 n_z H_\varphi^+(\rho,z)[-\hat{\boldsymbol{x}}]\Big]\mathrm{e}^{-\mathrm{j}kz}\rho\,\mathrm{d}\ell \\ &= \hat{\boldsymbol{x}}\frac{\mathrm{j}k}{4}\int_\gamma \Big[n_\rho E_z^+(\rho,z) - n_z E_\rho^+(\rho,z) + \eta_0 n_z H_\varphi^+(\rho,z) \\ &\quad - \mathrm{j}n_z E_\varphi^+(\rho,z) + \mathrm{j}\eta_0(n_\rho H_z^+(\rho,z) - n_z H_\rho^+(\rho,z))\Big]\mathrm{e}^{-\mathrm{j}kz}\rho\,\mathrm{d}\ell\end{aligned} \quad (3.22)$$

This demonstrates that we need to solve for only one mode, $m = 1$, and then compute the line integral above in order to find the far field amplitude for a linearly polarized incident plane wave.

In conclusion, the far field amplitude in the backscattering direction for an axially symmetric structure illuminated by a plane wave $E_0\mathrm{e}^{-\mathrm{j}kz}\hat{\boldsymbol{x}}$ is given by (dropping the "+" mode indicator for brevity)

$$\begin{aligned}\boldsymbol{F}(-\hat{\boldsymbol{z}}) = \hat{\boldsymbol{x}}\frac{\mathrm{j}k}{4}\int_\gamma \Big[&n_\rho E_z(\rho,z) - n_z E_\rho(\rho,z) + \eta_0 n_z H_\varphi(\rho,z) \\ &- \mathrm{j}n_z E_\varphi(\rho,z) + \mathrm{j}\eta_0(n_\rho H_z(\rho,z) - n_z H_\rho(\rho,z))\Big]\mathrm{e}^{-\mathrm{j}kz}\rho\,\mathrm{d}\ell\end{aligned} \quad (3.23)$$

where the field components $(E_\rho, E_\varphi, E_z, H_\rho, H_\varphi, H_z)$ are computed from the azimuthal mode $m = 1$ (all fields are multiplied by $\mathrm{e}^{-\mathrm{j}\varphi}$), using the excitation $\boldsymbol{E}_0 =$

$E_0 \mathrm{e}^{-\mathrm{j}kz}(\hat{\boldsymbol{\rho}} - \mathrm{j}\hat{\boldsymbol{\varphi}})$. The monostatic radar cross section is finally given by

$$\sigma = 4\pi \frac{|\boldsymbol{F}(-\hat{\boldsymbol{z}})|^2}{|E_0|^2} \tag{3.24}$$

In the following, we show how the electric and magnetic field components can be determined in the PO approximation.

## 3.2 Physical optics application

We now translate the general PO equations to the specific coordinate system for the axially symmetric case. The vectors $\hat{\boldsymbol{p}}$ and $\hat{\boldsymbol{s}}$ can then be identified as

$$\hat{\boldsymbol{p}} = \hat{\boldsymbol{\varphi}} \times \hat{\boldsymbol{n}} = n_z \hat{\boldsymbol{\rho}} - n_\rho \hat{\boldsymbol{z}} \tag{3.25}$$

$$\hat{\boldsymbol{s}} = \hat{\boldsymbol{\varphi}} \tag{3.26}$$

Projecting the incident field $\boldsymbol{E}^{(\mathrm{i})} = E_0 \mathrm{e}^{-\mathrm{j}kz}(\hat{\boldsymbol{\rho}} - \mathrm{j}\hat{\boldsymbol{\varphi}})$ on the TM and TE polarizations then implies

$$E^{(\mathrm{i})}_{\mathrm{TM}} = \hat{\boldsymbol{p}} \cdot \boldsymbol{E}^{(\mathrm{i})} = n_z E_0 \mathrm{e}^{-\mathrm{j}kz} \tag{3.27}$$

$$E^{(\mathrm{i})}_{\mathrm{TE}} = \hat{\boldsymbol{s}} \cdot \boldsymbol{E}^{(\mathrm{i})} = -\mathrm{j} E_0 \mathrm{e}^{-\mathrm{j}kz} \tag{3.28}$$

The expression for the far field amplitude can be rewritten in terms of TM and TE polarizations as well:

$$\begin{aligned} \boldsymbol{F}(-\hat{\boldsymbol{z}}) &= \hat{\boldsymbol{x}} \frac{\mathrm{j}k}{4} \int_\gamma \Big[ n_\rho E_z - n_z E_\rho + \eta_0 n_z H_\varphi - \mathrm{j} n_z E_\varphi + \mathrm{j}\eta_0 (n_\rho H_z - n_z H_\rho) \Big] \mathrm{e}^{-\mathrm{j}kz} \rho \, \mathrm{d}\ell \\ &= \hat{\boldsymbol{x}} \frac{\mathrm{j}k}{4} \int_\gamma \Big[ -\hat{\boldsymbol{p}} \cdot \boldsymbol{E} + \eta_0 n_z \hat{\boldsymbol{s}} \cdot \boldsymbol{H} - \mathrm{j} n_z \hat{\boldsymbol{s}} \cdot \boldsymbol{E} - \mathrm{j}\eta_0 \hat{\boldsymbol{p}} \cdot \boldsymbol{H} \Big] \mathrm{e}^{-\mathrm{j}kz} \rho \, \mathrm{d}\ell \end{aligned} \tag{3.29}$$

The explicit expressions are

$$\hat{\boldsymbol{p}} \cdot \boldsymbol{E} = (1 + R_{\mathrm{TM}}) n_z E_0 \mathrm{e}^{-\mathrm{j}kz} \tag{3.30}$$

$$\hat{\boldsymbol{s}} \cdot \boldsymbol{H} = -\frac{\eta_0^{-1}}{\cos\theta} (1 - R_{\mathrm{TM}}) n_z E_0 \mathrm{e}^{-\mathrm{j}kz} \tag{3.31}$$

$$\hat{\boldsymbol{s}} \cdot \boldsymbol{E} = (1 + R_{\mathrm{TE}})(-\mathrm{j} E_0 \mathrm{e}^{-\mathrm{j}kz}) \tag{3.32}$$

$$\hat{\boldsymbol{p}} \cdot \boldsymbol{H} = \eta_0^{-1} \cos\theta (1 - R_{\mathrm{TE}})(-\mathrm{j} E_0 \mathrm{e}^{-\mathrm{j}kz}) \tag{3.33}$$

Inserting into the far field expression implies

$$\begin{aligned} \boldsymbol{F}(-\hat{\boldsymbol{z}}) = -\hat{\boldsymbol{x}} \frac{\mathrm{j}k}{4} \int_\gamma \Bigg[ &(1 + R_{\mathrm{TM}}) n_z + \frac{1 - R_{\mathrm{TM}}}{\cos\theta} n_z^2 + (1 + R_{\mathrm{TE}}) n_z \\ &+ \cos\theta (1 - R_{\mathrm{TE}}) \Bigg] E_0 \mathrm{e}^{-2\mathrm{j}kz} \rho \, \mathrm{d}\ell \end{aligned} \tag{3.34}$$

which is the final result. All parameters inside the integral can be parametrized along the curve $\gamma$. It is immediately seen that sections of a straight circular cylinder, where $n_z = 0$ and $\cos\theta = 0$, give zero contribution regardless of the reflection coefficients.

# 4 Simulation results

## 4.1 Monostatic RCS on axis

The PO expression in (3.34) was implemented in a Python script, using the SciPy package for scientific computing [13], to determine the monostatic RCS from a capped cylinder scatterer as in Figure 2. The PO implementation was benchmarked by simulating the same geometry in Comsol Multiphysics axially-symmetric finite element method (FEM) solver. The FEM solver in Comsol was benchmarked against the method of moments (MoM) solver in FEKO, and the results are presented in Appendix A. The radius of the scatterer was defined as $a$, and the length of the scatterer $L_{\text{tot}} = L + a$, where $L = 3a$ and $a = 8.4\lambda_0/(2\pi)$ or $a = 17.4\lambda_0/(2\pi)$, respectively in the two different geometries under study. The PO parametrization of the geometry was carried out explicitly by breaking down the geometry to three regions:

| | Semisphere | Straight cylinder | Flat top |
|---|---|---|---|
| $u$ | $0 < u < 1/3$ | $1/3 < u < 2/3$ | $2/3 < u < 1$ |
| $\rho$ | $a\sin(u3\pi/2)$ | $a$ | $a - (3u-2)a$ |
| $z$ | $-L/2 - a\cos(u3\pi/2)$ | $-L/2 + (3u-1)L$ | $L/2$ |
| $\hat{\boldsymbol{n}}$ | $\sin(u3\pi/2)\hat{\boldsymbol{\rho}} - \cos(u3\pi/2)\hat{\boldsymbol{z}}$ | $\hat{\boldsymbol{\rho}}$ | $\hat{\boldsymbol{z}}$ |
| $\mathrm{d}\ell/\,\mathrm{d}u$ | $a3\pi/2$ | $3L$ | $3a$ |
| $\cos\theta$ | $\cos(u3\pi/2)$ | $0$ | $-1$ |

The angle of incidence is in this case given by

$$\cos\theta = -\hat{\boldsymbol{z}} \cdot \hat{\boldsymbol{n}}(u) = \frac{\rho'(u)}{\sqrt{(z'(u))^2 + (\rho'(u))^2}} \tag{4.1}$$

Here, it is clearly seen that the straight part of the cylinder and the flat top do not satisfy $\cos\theta > 0$, and hence are in the shadow region in the PO approximation. The simulation in Comsol was carried out using 10 steps per wavelength mesh setting for the highest frequency of the simulation, and the monostatic RCS was evaluated at 501 frequency points. In the PO implementation, the monostatic RCS was evaluated at 1001 points along the curve $\gamma$ defining the scatterer for 1001 frequency points.

A comparison of the results is presented in Figure 3, where it can be seen that the PO curves appear to roughly correspond to the average of the oscillating full wave simulation curves. The PO curves agree well with the full wave results for a PEC scatterer, but when the structure is coated by a Salisbury absorber as in Figure 5 the curves deviate for the frequencies of operation of the absorber. This effect is explained in Figure 4, where the simulation data from Comsol in the right plot in Figure 3 has been gated in time domain using the window function in the left plot in Figure 4. The result of this operation is that the scattering from the back edge of the object is removed. It can be seen in the right plot in Figure 4 that now

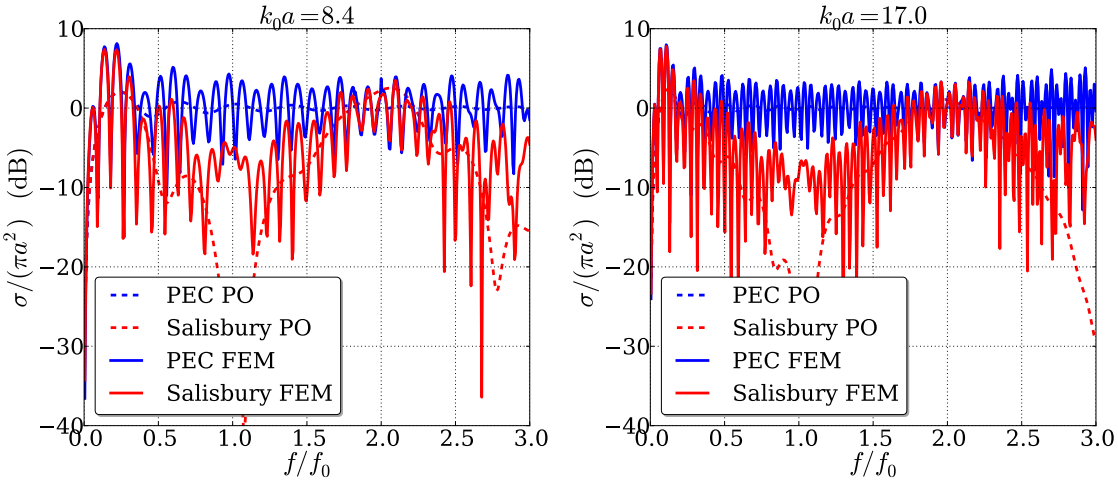


Figure 3: Comparison between simulation results of a capped cylinder in Comsol and in the PO implementation. The dashed curves correspond to the monostatic RCS from the PO implementation and the solid curves correspond to simulation results from Comsol. In the left plot the radius of the hemispherical cap of the scatterer is $a = 8.4\lambda_0/(2\pi)$ and in the right plot $a = 17\lambda_0/(2\pi)$.

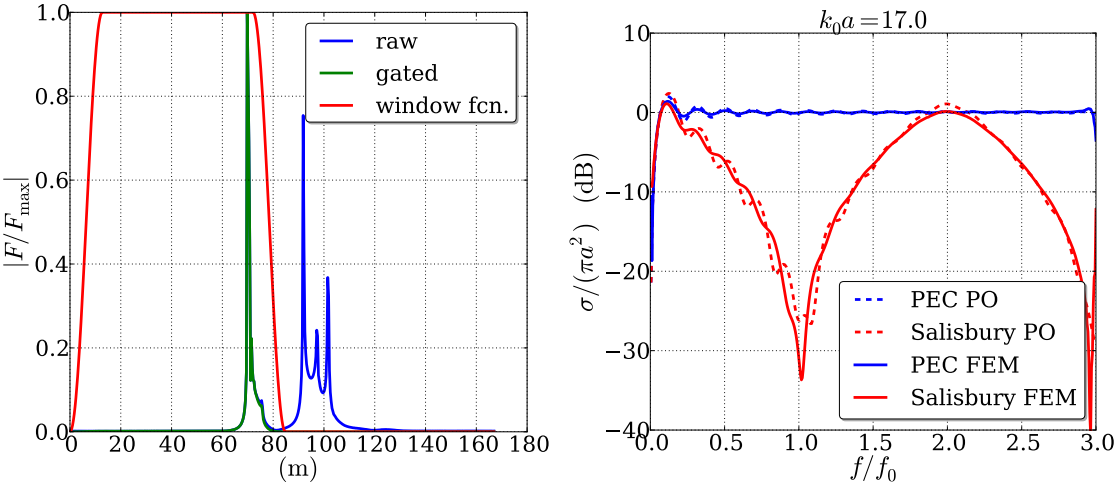


Figure 4: Comparison between simulation results of a capped cylinder in Comsol and in the PO implementation. The dashed curves correspond to the monostatic RCS from the PO implementation and the solid curves correspond to simulation results from Comsol. In the right plot the Comsol RCS data have been gated in time domain using the window function in the left figure, which implies that the scattering from the back of the object has been filtered out. The radius of the hemispherical cap of the scatterer is $a = 17\lambda_0/(2\pi)$.

the agreement is much better between the PO data and the full wave simulation data from Comsol.

Next, a hemispherically capped cylinder as in Figure 2 with $L = 30\lambda_0$ and $a = 10\lambda_0$ or $a = \lambda_0$ was simulated in the PO solver for three different scenarios: a PEC structure, and the structure covered with either a Dallenbach absorber or a

Salisbury absorbers, where the absorbers were designed to have their primary operation at $f_0 = c_0/\lambda_0$ (meaning they have approximate thickness $\lambda_0/4$). In Figure 5 the absorbers and their material parameters are presented and the reflection coefficients for the absorbers are shown in Figure 6. The resulting normalized RCS are shown in Figure 7.

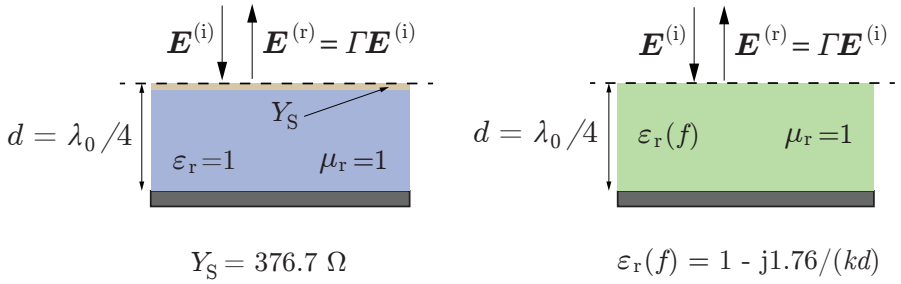


Figure 5: Electromagnetic absorbers simulated in this work. To the left is a Salisbury screen[19] and to the right is a DÃd'llenbach absorber, designed to have a deep null at $f_0 = c/\lambda_0$. Both absorbers have the thickness $\lambda_0/4$.

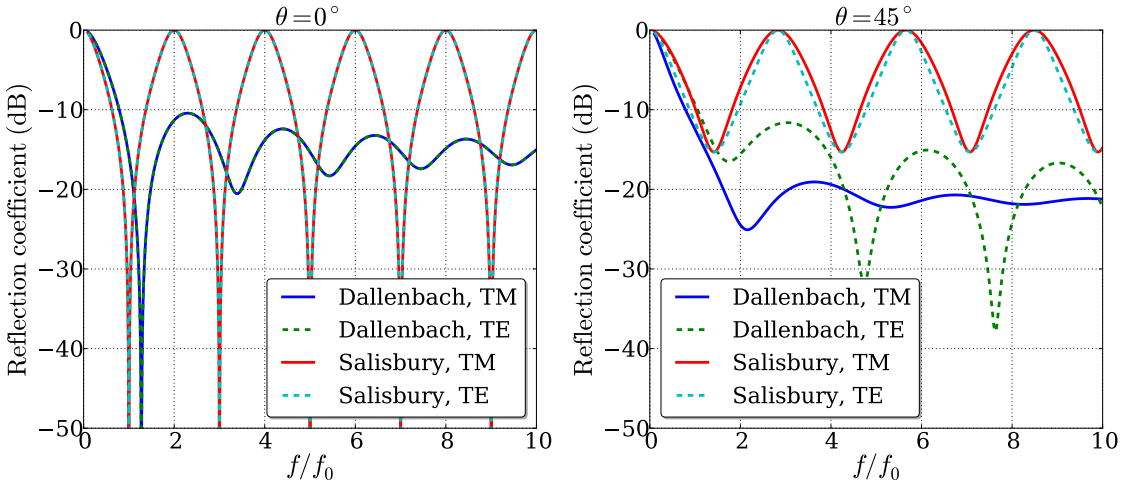


Figure 6: Typical reflection coefficients from the different absorbers.

## 4.2 Monostatic RCS off axis

In order to characterize the monostatic RCS when illuminating a scatterer in a direction offset to the axis of rotation of the object, the general PO expression of the monostatic far field in (2.9) was implemented in Python. The hemispherically capped cylinder in Figure 2 was again simulated, this time for normal incidence(along the cylinder axis) and at a 10° offset. The dimensions were $L = 30\lambda_0$ and $a = \lambda_0$, where $\lambda_0$ is the design frequency for an absorbing layer. Some results are given in Figure 8, the monostatic RCS is evaluated at 200 frequency points, using 400, 800 or 1600 evaluation points of the integrating variables $u$ and $v$, respectively. It is seen that the discretization is a critical parameter to obtain accurate results. Using a high resolution (1600 evaluation points over the surface that is integrated), the RCS for the offset angle of incidence is comparable to that of normal incidence. This indicates that the errors caused by a coarse spatial sampling have been reduced.

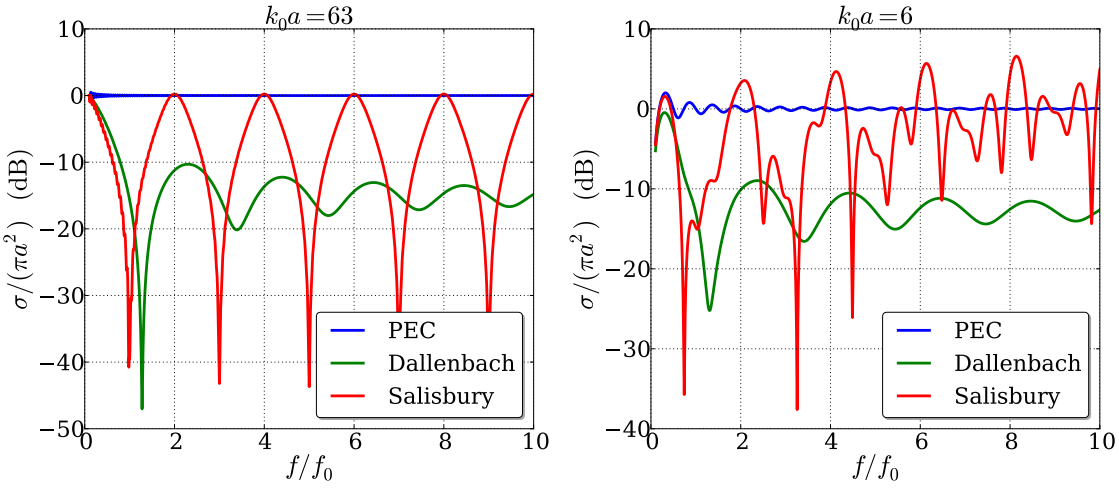


Figure 7: Left: results for a hemispherically capped cylinder with $L = 30\lambda_0$ and $a = 10\lambda_0$. Right: results for a hemispherically capped cylinder with $L = 30\lambda_0$ and $a = \lambda_0$.

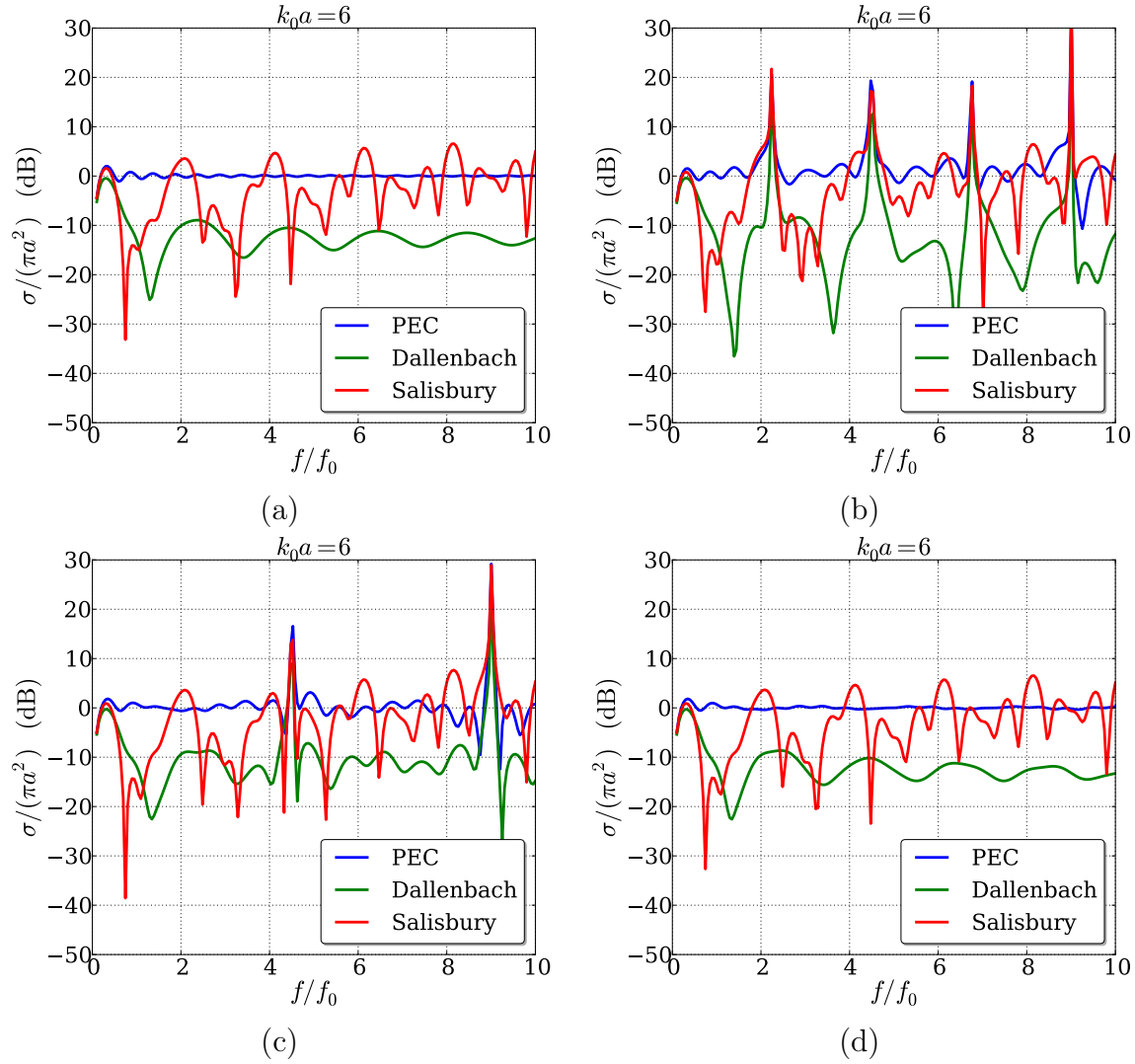


Figure 8: Radar cross section for a hemispherically capped cylinder. (a) Incidence along the cylinder axis. (b) Incidence offset 10° relative the cylinder axis, polarization in the plane spanned by cylinder axis and direction of incidence. (c) Same as (b), with double resolution. (d) Double the resolution of (c).

# 5 Conclusions

We have demonstrated a specialized method to compute the far field amplitude, and subsequently the monostatic radar cross section, for an axially symmetric object subject to an incident wave along the cylinder axis. The resulting expression can be used in a full wave simulator like Comsol, or for very fast computations in a physical optics approximation. An initial implementation was demonstrated for two simple absorbers on a hemispherically capped cylinder structure. A general PO expression was also formulated for calculating the scattering from an arbitrary 3D surface, and it was applied to a rotational symmetric structure.

# A Full Wave Benchmark Simulations and Mesh Convergence

A hemispherically capped cylinder with the parameters $a = 4\lambda_0/3$, $L_{\text{tot}} = 16\lambda_0/3$, $w = 8\lambda_0/3$ was simulated both in FEKO and in the 2D axially symmetric solver in Comsol Multiphysics for verification of the integral expression (3.23). The structure was simulated both with and without a Salisbury absorber and the results in Figure 9 show good agreement between the softwares. In the right plot in Figure 9 a mesh convergence study from Comsol Multiphysics is presented, where a PEC capped cylinder of the same size as in the left plot has been simulated using different mesh settings. It can be seen that when 10 steps per wavelength (at the shortest wavelength of the simulation $\lambda_2$) mesh setting is used, the agreement is good in comparison to much finer mesh settings.

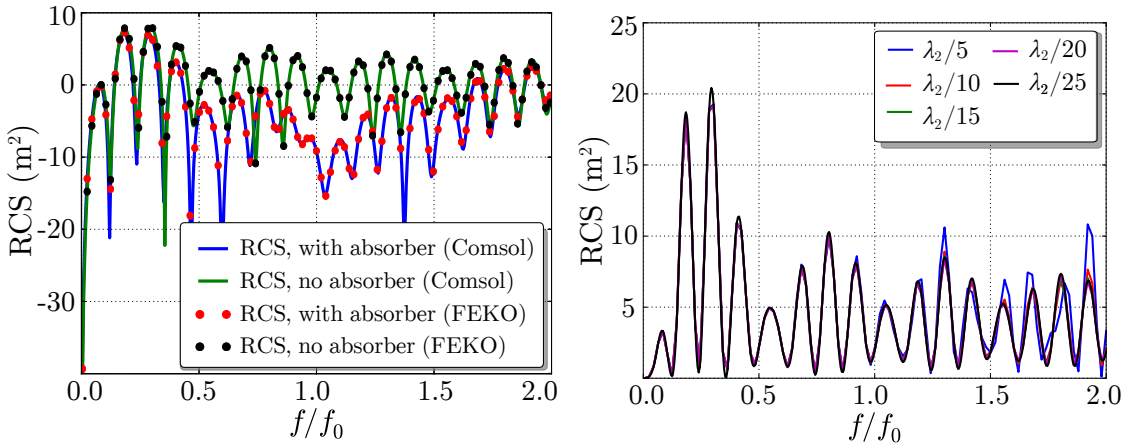


Figure 9: In the left figure a capped cylinder with the radius $a = 4\lambda_0/3$, length $L_{\text{tot}} = 16\lambda_0/3$ and width $w = 8\lambda_0/3$ has been simulated both in FEKO and in Comsol Multiphysics, using 10 steps per wavelength mesh setting, with and without a Salisbury screen absorber applied. In the right figure a PEC capped cylinder scatterer has been simulated in Comsol using different mesh settings.

# References

[1] F. S. de Adana, I. G. Diego, O. G. Blanco, P. Lozano, and M. F. Catedra. "Method based on physical optics for the computation of the radar cross section including diffraction and double effects of metallic and absorbing bodies modeled with parametric surfaces". *IEEE Transactions on Antennas and Propagation* 52 (12) (2004): pp. 3295–3303.

[2] S. A. Akhmanov and S. Y. Nikitin. "Physical optics". Clarendon Press, 1997.

[3] A. Boag. "A fast physical optics (fpo) algorithm for high frequency scattering". *IEEE Transactions on Antennas and Propagation* 52 (1) (2004): pp. 197–204.

[4] A. Boag and C. Letrou. "Multilevel fast physical optics algorithm for radiation from non-planar apertures". *IEEE Transactions on Antennas and Propagation* 53 (6) (2005): pp. 2064–2072.

[5] M. Born and E. Wolf. "Principles of optics: electromagnetic theory of propagation, interference and diffraction of light". Elsevier, 2013.

[6] D. B. Davidson. "Computational electromagnetics for RF and microwave engineering". Cambridge University Press, 2005.

[7] A. Ericsson, D. Sjöberg, C. Larsson, and T. Martin. *Approximative computation methods for monostatic scattering from axially symmetric objects*. Tech. rep. LUTEDX/(TEAT-7256)/1–XX/(2017). Lund Institute of Technology, 2017.

[8] A. Ericsson, D. Sjöberg, C. Larsson, and T. Martin. *Scattering from a multilayered sphere - Applications to electromagnetic absorbers on double curved surfaces*. Tech. rep. LUTEDX/(TEAT-7249)/1–33/(2017). Lund Institute of Technology, 2017.

[9] A. Ericsson, D. Sjöberg, C. Larsson, and T. Martin. "Scattering for doubly curved functional surfaces and corresponding planar designs". In: *Antennas and Propagation (EuCAP), 2016 10th European Conference on*. IEEE. 2016, pp. 1–2.

[10] M. Ferrando-Bataller, F. V. Bondìa, and A. Valero-Nogueira. "Fast physical optics for smooth surfaces". In: *Proceedings of the Fourth European Conference on Antennas and Propagation*. 2010, pp. 1–3.

[11] A. Gendelman, Y. Brick, and A. Boag. "Multilevel physical optics algorithm for near field scattering". *IEEE Transactions on Antennas and Propagation* 62 (8) (2014): pp. 4325–4335.

[12] J. M. Jin. "Theory and Computation of Electromagnetic Fields". Wiley, 2011.

[13] E. Jones, T. Oliphant, P. Peterson, et al. *SciPy: Open source scientific tools for Python*. 2001.

[14] E. F. Knott, J. F. Shaeffer, and M. T. Tuley. "Radar Cross Section". SciTech Publishing Inc., 2004.

[15] G. Kristensson. "Scattering of Electromagnetic Waves by Obstacles". SciTech Publishing, an imprint of the IET, 2016.

[16] C. Letrou and A. Boag. "Generalized multilevel physical optics (mlpo) for comprehensive analysis of reflector antennas". *IEEE Transactions on Antennas and Propagation* 60 (2) (2012): pp. 1182–1186.

[17] E. Michielssen and A. Boag. "Multilevel evaluation of electromagnetic fields for the rapid solution of scattering problems". *Microwave and Optical Technology Letters* 7 (17) (1994): pp. 790–795.

[18] K. Mitzner. *Incremental length diffraction coefficients*. Tech. rep. DTIC Document, 1974.

[19] B. Munk. "Frequency Selective Surfaces: Theory and Design". John Wiley & Sons, 2000.

[20] G. T. Ruck, D. E. Barrick, W. D. Stuart, and C. K. Krichbaum. "Radar Cross-Section Handbook". Vol. 1 and 2. Plenum Press, 1970.

[21] T. Shijo, L. Rodriguez, and M. Ando. "The modified surface-normal vectors in the physical optics". *IEEE Transactions on Antennas and Propagation* 56 (12) (2008): pp. 3714–3722.

[22] D. G. Smith. "Field Guide to Physical Optics". SPIE Press, 2013.

[23] O. N. Stavroudis. "The Mathematics of Geometrical and Physical Optics: the k-function and its Ramifications". John Wiley & Sons, 2006.

[24] P. Y. Ufimtsev. *Method of edge waves in the physical theory of diffraction*. Tech. rep. DTIC Document, 1971.

[25] P. Y. Ufimtsev. "Fundamentals of the physical theory of diffraction". John Wiley & Sons, 2007.

[26] Y. Z. Umul. "Modified theory of physical optics". *Opt. Express* 12 (20) (2004): pp. 4959–4972.

[27] C. Wang, Y. Wang, S. Wu, X. Liu, and S. Sun. "An effective rcs calculation technique for composite coated targets". In: *2015 IEEE International Symposium on Antennas and Propagation USNC/URSI National Radio Science Meeting*. 2015, pp. 766–767.